MedChemComm

RESEARCH ARTICLE

View Article Online
View Journal | View Issue

Cite this: *Med. Chem. Commun.*, 2017, **8**, 2055

Cancer nanomedicine: from PDGF targeted drug delivery†

Chandrababu Rejeeth, *[a] Raju Vivek,[a] Varukattu NipunBabu,[b] Alok Sharma,[a] Xianting Ding[a] and Kun Qian*[a]

Received 31st July 2017,
Accepted 28th September 2017

DOI: 10.1039/c7md00391a

rsc.li/medchemcomm

An innovative approach for the distinctively efficient action of smart targeted drug delivery to a specific cell type is obtained through the modification of the surface of nanoparticles. Specifically, the work identifies a cell surface receptor targeting drug delivery nanosystem based on mesoporous silica loaded with the anti-cancer drug cisplatin (*cis*-DDP) and poly-acrylic acid (PAA). A specific target is the PDGF receptors expressed in cervical cancer cells, thus making the PAA functionalized nanocomposite a suitable and promising nano-medicine for the targeting of PDGF-overexpressing cancers in the near future.

Nanoparticles (NPs) have been established as an imperative approach for therapeutic and diagnostic purposes of imaging, metabolic analysis and profiling of serum biomarkers *via* ligand–protein interactions.[1–5] Because nanoparticles are efficient in delivering a highly potent dose of these agents to a target site with conserved activity of the agents during transit in the blood stream.[6] Cancers constitute a dynamic environment including various cell types such as epithelial cells, fibroblasts, endothelial cells, stromal cells, and inflammatory cells such as macrophages. Efficient and site-specific delivery of therapeutic drugs is a critical challenge in the clinical treatment of cancer.[7] Typically, NPs conjugate their surface with cancer-specific targeting motifs like antibodies or short peptides that exhibit high affinity towards cancer-specific antigens or receptors, *e.g.* folate receptors and endothelial growth factor receptors.[7,8] Furthermore, NPs associate with cells through one of the traditional pathways: specifically, macropinocytosis, clathrin-mediated endocytosis,[9] and caveolae-mediated endocytosis.[10] Moreover, arginine-rich peptides (*e.g.*, cell penetrating peptides), which can create a new pore on the cell membrane, enable direct translocation of the NPs into cytosol.[11] Several distinct factors influence the uptake into cells, like size, shape, and surface charge.[12] It is well known that positively charged NPs are well suited to the endocytic treatment of cells as they can interact with the negatively charged lipid components of the cell membrane.[13] The assistance of NP surface chemistry on cell–NP interactions and cellular uptake is being accepted.[14] Accordingly, our understanding of the role of the physico-chemical characteristics of NPs in cellular uptake is quite limited. One of the challenges associated with using disease-based targets for homing of a therapeutic agent is the variability in expression of targets due to patient–patient variability and the stage of the tumor. Therefore, an extremely universal approach that can differentiate between various types of cell created within a cancer environment without the necessity for receptor-based targeting could be of value. Therefore, we ask the question: would it be possible to target a specific cell type *via* the physico-chemical characteristics of a nano-carrier? From a biophysical viewpoint, receptor–ligand interactions can be distilled down to an interplay and balance between hydrophobic and electrostatic interactions. Here, we applied a simple premise; we theorized that an MSNs@*cis*-DDP@PAA system possessing two characteristics, (i) a high affinity for the cell membrane and (ii) a highly negatively charged surface, will diminish nonspecific charge–charge interactions between the NPs and cell surface, thereby promoting affinity-based interactions with the cell surface, thus enabling the targeting of cell domains. To assess the selectivity, platelet-derived growth factor (PDGF) (14.4 kDa, pI = 9.4) was selected as a competing, positively charged model cell surface receptor. PDGF signalling pathways contribute to the pathogenesis of many diseases including cancer. Moreover, we find some early reports of PAA and PDGF biomarker binding efficiency,[15,16] and release functional platelet-derived growth factor-BB (PDGF-BB) to induce *in vivo* localized neovascularization.[17] To the best of our knowledge no PDGF guided nano-drug delivery for the treatment of PDGF expressing cancer cells has been reported. We claim the first prodrug-based MSN (mesoporous silica nanoparticle) delivery system which has cisplatin conjugated on the surface of the MSNs coated with PAA through reducible linkages, which is taken up by endothelial cells without the need for cell-specific targeting ligands. To further investigate the application of NPs in

[a] *Department of Biomedical Engineering, MED-X Research Institute, Shanghai Jiao Tong University, Shanghai 200030, People's Republic of China.*
E-mail: crejee@gmail.com, crejee@sjtu.edu.cn, k.qian@sjtu.edu.cn
[b] *Proteomics & Molecular Cell Physiology Laboratory, Department of Zoology, School of Life Sciences, Bharathiar University, Coimbatore 641 046, Tamilnadu, India*

† Electronic supplementary information (ESI) available. See DOI: 10.1039/c7md00391a

chemotherapy the relationships among NP surface physicochemical characteristics, cell surface domains and NP systems that can inherently discriminate between healthy and diseased cells may be realized in the near future.

Versatile MSNs, with the cisplatin prodrug conjugated to the inner pores of the MSN surface and made electrostatically repulsive with an affinity probe (PAA), were synthesized *via* a multistep procedure as depicted in Scheme S1.† A schematic presentation of the distribution process of the drug loaded MSNs@*cis*-DDP@PAA is shown in Scheme 1. Here, to gain a better understanding of the size dependent binding of PAA-MSNs to PDGF, a series of PAA-GNP was synthesized as previously reported,[18,19] and used to characterize their molecular interactions with human fibrinogen. The PAA-MSNs bound to PDGF with saturating kinetics are shown in Fig. S1.† We believe that this was caused by the peculiar interplay of the PAA-MSNs and their increased sizes as shown in Fig. S2.†

The typical TEM image is shown in Fig. 1, and it can be seen that the MSNs have a well-ordered mesoporous structure. The mean particle sizes are estimated to be 60–100 nm. Fig. 1a shows the representative TEM image of the MSNs. A TEM image of the drug loaded MSNs@*cis*-DDP@PAA system shows well-dispersed nanoparticles, while the mesoporous channels are not as clear which indicates the successful inner surface coating with the cisplatin prodrug and affinity probe, as shown in Fig. 1b. Meanwhile, Fig. 1c shows the zeta potential of the MSNs, MSNs@NH_2, MSNs@*cis*-DDP and MSNs@*cis*-DDP@PAA nanocomposites with charges of −22.3, +20.3, +15.8 and −26.4 mV respectively, which are consistent with the modification of amine groups (MSNs@NH_2) on the negatively charged silica surface (MSNs) and the subsequent conjugation of the cisplatin prodrug on the positively charged MSNs@NH_2 due to the carboxylic group of the prodrug. The

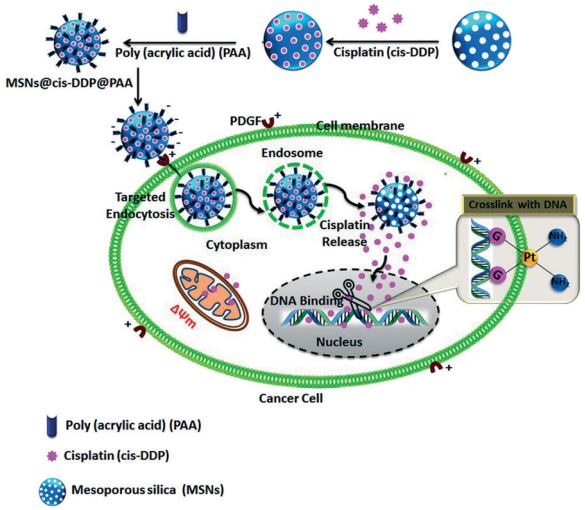

Scheme 1 A schematic representation of the fabrication, the mode of electrostatic interactions between a PAA modified negative nanocomposite and a cell membrane which can promote highly specific interactions with the cell membrane leading to uptake that is dominated by electrostatic attraction, and the mechanism of the intercellular delivery system.

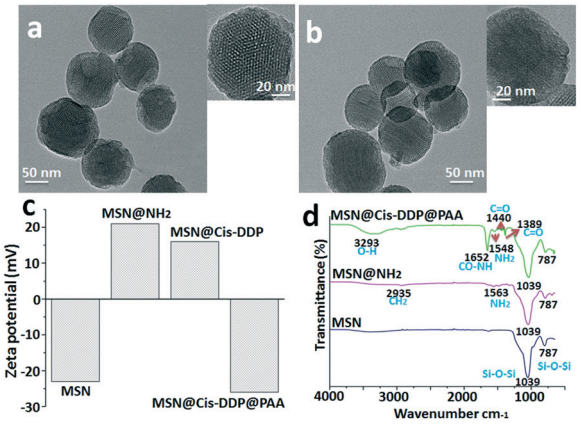

Fig. 1 Instrumental analysis of the MSN nanocomposites: (a) TEM characterization of the bare MSNs, (b) a TEM image of MSNs@*cis*-DDP@PAA, (c) zeta potential changes for the MSNs, MSNs@NH_2, MSNs@*cis*-DDP and MSNs@*cis*-DDP@PAA and (d) an FTIR spectrum of the MSNs, MSNs@NH_2, and MSNs@*cis*-DDP@PAA.

MSNs@*cis*-DDP complex has an NH_3^+ group on the surface and the PAA surface has an –OH group which both electrostatically connect, but the unreacted carboxylic groups support the binding with the positively charged receptor. As shown in Fig. 1d, the MSNs exhibit a broad peak for the Si–O–Si stretching bond at 787–1039 cm^{-1}, and after amine modification the MSNs@NH_2 show a shoulder peak at around 2933 cm^{-1} associated with –CH_2, and a peak for the CO–NH_2 (amide) bond at 1563 cm^{-1}. MSNs@*cis*-DDP@PAA exhibit a typical bond peak at 3293 cm^{-1} (O–H) from PAA.[20] The characteristic peaks at 787 and 1039 cm^{-1} for MSNs@PAA can be indexed to Si–O–Si stretching. In addition, a shoulder peak at 1548 cm^{-1} can also be observed for MSNs@NH_2, which can be attributed to the stretching mode of Si–O in the Si–NH group. A band at 1389–1440 cm^{-1} with a peak is observed for MSNs@*cis*-DDP which is assigned to the bending mode.[21] The results show that *cis*-DDP and PAA have been successfully conjugated on the MSNs. EDX spectra of the MSNs were obtained, as shown in Fig. S3a&b,† and typical Pt peaks were clearly observed, which confirmed the successful conjugation of the cisplatin prodrug. Subsequently, the amount of Pt on the MSNs was determined by ICP-MS to be ~4.0% (w/w).[21] The nitrogen adsorption–desorption plot of the MSNs shown in Fig. S3d† exhibits a typical type BJH isotherm and a steep capillary condensation step occurring at a relative pressure (P/P_0) of ~0.45, corresponding to a narrow pore size distribution of 5–15 nm (Fig. S3c†). The surface area and pore volume are calculated to be 980.5 $m^2\ g^{-1}$ and 0.76 $cm^3\ g^{-1}$ respectively. The surface modification of the MSNs has been studied by zeta potential, FTIR, and ^{1}H NMR analysis. The ^{1}H NMR solid-state spectra of MSNs@NH_2 and MSNs@PAA are presented in Fig. S4.† The sharp peaks observed at about 0.33 ppm in the spectrum of MSNs@NH_2 can be assigned to methylene carbons from the amino-silica source in Fig. S4a.† The peaks in the range 1.01 ppm can be attributed to carbons and the carboxylate carbons of the PAA polymer observed in the spectrum of MSNs@PAA. The results

show that PAA has been successfully conjugated on MSNs@PAA, as shown in Fig. S4b.†

As described previously, bare *cis*-DDP shows low anticancer effect due to low cellular uptake. Therefore, the effort of our work has been directed to increase the effect of cisplatin through conjugation to MSNs@PAA. The cellular internalization and intracellular distribution of MSNs@*cis*-DDP@PAA/Ce6 in HeLa cells were evaluated by confocal laser scanning microscopy (CLSM) to monitor the time-dependent intracellular behaviour of the drug delivery system. An Invitrogen probe, LysoTracker Green (LTG), was used to stain the acidic organelles in the HeLa cells. We found that MSNs@*cis*-DDP@PAA/Ce6 dominantly localized in the LTG-labelled acidic organelles after 6 h incubation. The red fluorescence (Ce6-red) of MSNs@*cis*-DDP@PAA/Ce6 mostly separated from the green fluorescence of LTG and located in the cytoplasm, indicating the successful escape of the nanoparticles from the lysosome,[22] as shown in Fig. 2a. The *cis*-DDP release profiles were obtained for the MSNs@*cis*-DDP nanoparticles and the MSNs@*cis*-DDP@PAA nanocomposite at pH values of 5 and 7.4. Considering the acidic environment of cancer cells, the pH value of a phosphate buffer solution for *in vitro* drug release was chosen to be 5.0 in this experiment. Just as we expected, the *cis*-DDP release rate of the MSNs@*cis*-DDP@PAA nanocomposite is slower than that of the MSNs@*cis*-DDP nanoparticles, due to the presence of the mesoporous silica, through which *cis*-DDP is released from the carrier. This process is a typical diffusion-controlled process, with the *cis*-DDP release behaviour of the nanocomposite being further influenced by the pore channels of the silica as well as the cleavage of the amide bonds.[23] In addition, due to the pH dependence of the cleavage of the amide bonds and the presence of the mesoporous silica, the *cis*-DDP release rate of the synthesized MSNs@*cis*-DDP@PAA is much slower under physiological conditions (Fig. 2b). Thus the prepared drug delivery nanoparticles are expected to act as an intracellular depot and to promote sustained drug retention. Rapid dissociation of the drug from the nanoparticles may result in its premature release into the blood stream, significantly reducing the efficient delivery of the drug molecules to the desired tissue/organ and it being retained there for a sustained period of time. To estimate whether MSN conjugation exerts any influence on the drug, the effects of *cis*-DDP and the MSNs@*cis*-DDP and MSNs@*cis*-DDP@PAA drug conjugates were evaluated by calculating cell toxicity using an MTT assay with various concentrations (0–90 μg mL^{-1}) of HeLa (PDGF+) and A549 (PDGF−) cancer cell lines. As expected, *cis*-DDP showed moderate cell toxicity in the HeLa cell line as showed in Fig. S5.† MSNs@*cis*-DDP showed less cell toxicity which might be explained by the depressed cellular uptake and lots of leakage in the cellular system. However, as expected, MSNs@*cis*-DDP@PAA showed an enhanced drug effect compared to *cis*-DDP and MSNs@*cis*-DDP. In the case of HeLa cells, the higher levels of PDGF expression on the cell surface allow the PAA modified nanocomposite to easily bind with the PDGF receptors leading to endocytosis and a significantly higher cytotoxicity in HeLa cells compared to that in A549 cells because cellular binding efficiency is very low (see ESI† Fig. S2).

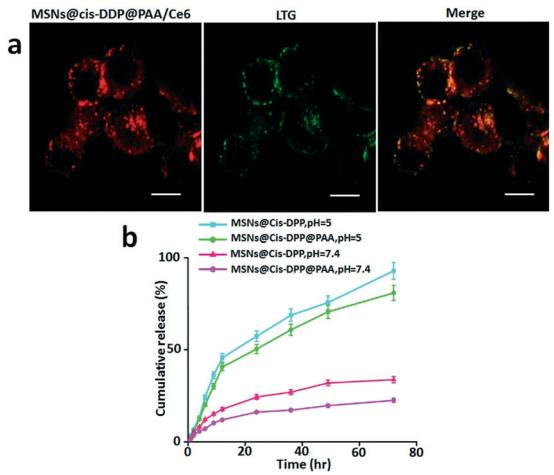

Fig. 2 Intracellular trafficking of the MSNs@*cis*-DDP@Ce6@PAA nanocomposite in HeLa cells. (a) Confocal microscopy images of HeLa cells labelled with LysoTracker Green (LTG). HeLa cells were incubated with the MSNs@*cis*-DDP@PAA/Ce6 nanocomposite (50 μg mL^{-1}) for the indicated times and then stained with LTG (150 nM, 30 min). The red fluorescence is from Ce6 inside the nanocomposite under 405 nm excitation, and the green fluorescence is from LTG under 488 nm excitation. (b) The *cis*-DDP release profiles from the MSNs@*cis*-DDP and MSNs@*cis*-DDP@PAA nanocomposites at pH 5 and 7.4 with a temperature maintained at 37 °C.

All this evidence strongly suggests that the effective antitumor activity can be attributed to the *cis*-DDP released from the carriers into the cells. The MSNs@*cis*-DDP@PAA nanocomposite can be internalized by the cells through an endocytosis process, evidenced from the obvious fluorescence of FITC observed in the cytoplasm around the nuclei (blue, stained with DAPI) after FITC-labelled nanoparticles were incubated with HeLa cells for 0–6 hours (Fig. 3). To improve target specificity, as discussed above, the drug carrier system can also be easily functionalized with a targeting ligand *via* a silicone coupling agent.[24] Here, PAA was selected to modify the porous drug carrier system *via* 3-aminopropyltriethoxysilane (APTES) for increased and specific uptake of the drug carrier in tumour cells overexpressing the PDGF receptor, such as HeLa cells. Fig. 3 shows bright field and merged images of HeLa (high level of PDGF expression) cells, incubated with the MSNs@*cis*-DDP@PAA nanocomposite functionalized with PAA for 0–6 hours. Much stronger fluorescence was seen in the HeLa cells after 6 hours suggesting a specific uptake of the PAA modified mesoporous drug carrier system by the cells with PDGF receptors. These results indicate that the MSNs@*cis*-DDP functionalized with PAA is preferentially internalized by the cells *via* a receptor-mediated endocytosis process. The endosomes then fuse with low pH lysosomes to cleave the amide bonds between *cis*-DDP and the particles, allowing *cis*-DDP to be released first from the MSN surface and then to enter *via* the pore channels into the nucleus of the target cell where it exhibits

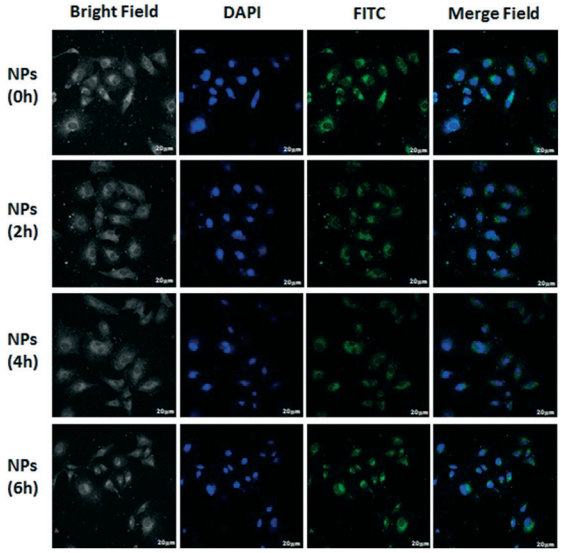

Fig. 3 The fluorescence of A549 cells incubated with MSNs@*cis*-DDP@PAA (*cis*-DDP equivalent concentration is 0.5 μg mL^{-1}) for 0–6 h. Images of nuclei stained with FITC (green colour) and DAPI (blue colour) were recorded. The scale bar is 20 μm.

antitumor activity. Fig. S6† shows bright field and merged images of A549 (low level of PDGF expression) and there are no differences in 0–6 h.

Finally, we provide a quantitative analysis of this phenomenon. We developed a technique for identifying individual mitochondria within a field of HeLa cell bodies and processes as shown in Fig. S7.† HeLa cells were incubated with the MSNs@*cis*-DDP@PAA nanocomposites for 0–6 hours and data were collected using the potentiometric dye JC-1. JC-1 was preferred for these experiments because its aggregates accumulate within functional mitochondria and make it fluorescent. This phenomenon allowed us to use the aggregate fluorescence signal to locate individual mitochondria and the monomer signal to detect changes in $\Delta\Psi_m$. A loss of $\Delta\Psi_m$ results in an increase in JC-1 monomer fluorescence in the regions in and around the mitochondria. These large regions of fluorescence, most typically seen in cell bodies, were excluded from the analysis based on size. This mechanism is induced by endoplasmic reticulum (ER) stress, causing a mitochondrial Ca^{2+} and Bcl-2 associated X protein (BAX) uptake, which will be followed by the loss of $\Delta\Psi_m$ and cytochrome-c and ATP release, building the apoptosomes. Certainly, the cellular inhibitory effect of the MSNs@*cis*-DDP@PAA nanocomposite in HeLa (high level of PDFG expression) cells was studied using nuclear staining with DAPI. The complex at a concentration of 10 mM showed characteristic apoptotic structures such as reduced and fragmented chromatin after 0–6 hours of treatment (Fig. S8†).

Conclusions

Traditional NP targeting with cell surface ligands using the lock and key principle offers specificity but is sensitive to the conformation and expression of these biological targets. The model shift presented in this study, which is based on exploiting the physicochemical characteristics of polymers (PAA) to engage specific cell surface motifs, offers unique possibilities for the discovery of unique cell surface targets for targeted nanomedicine. Our findings clearly show that synthetic polymers (PAA) can exhibit high specificity to a cell transporter domain that is critical in the regulation of movement of information in and out of cells, which provides a unique avenue for targeting and transport of payload into cells. Further studies are necessary to fully exploit the findings presented herein and achieve clinical translation.

Conflicts of interest

The authors declare no competing interests.

Acknowledgements

The authors gratefully thank the National Natural Science Foundation of China (NSFC) for financial support (No. 81550110257).

Notes and references

1 J. Wu, X. Wei, J. Gan, L. Huang, T. Shen, J. Lou, B. Liu, J. X. J. Zhang and K. Qian, *Adv. Funct. Mater.*, 2016, **26**, 4016–4025.
2 B. Liu, Y. Li, H. Wan, L. Wang, W. Xu, S. Zhu, Y. Liang, B. Zhang, J. Lou, H. Dai and K. Qian, *Adv. Funct. Mater.*, 2016, **26**, 7994–8002.
3 L. Huang, J. Wan, X. Wei, Y. Liu, J. Huang, X. Sun, R. Zhang, D. D. Gurav, V. Vedarethinam, Y. Li, R. Chen and K. Qian, *Nat. Commun.*, 2017, **8**, 220.
4 C. Rejeeth, X. Pang, R. Zhang, W. Xu, X. Sun, B. Liu, J. Lou, J. Wan, H. Gu, Y. Yan and K. Qian, *Nano Res.*, 2017, DOI: 10.1007/s12274-017-1591-6.
5 X. Sun, J. Wan and K. Qian, *Small Methods*, 2017, 1700196.
6 O. C. Farokhzad and R. Langer, *ACS Nano*, 2009, **3**, 16–20.
7 B. Yu, H. C. Tai, W. Xue, L. J. Lee and R. J. Lee, *Mol. Membr. Biol.*, 2010, **27**, 286–298.
8 H. Li, C. Liu, Y. P. Zeng, Y. H. Hao, J. W. Huang, Z. Y. Yang and R. Li, *ACS Appl. Mater. Interfaces*, 2016, **8**, 31510–31523.
9 D. Wang, L. Hu, M. Su, J. Wang and T. Xu, *Int. J. Oncol.*, 2015, **47**, 1160–1168.
10 S. Kumari, M. G. Swetha and S. Mayor, *Cell Res.*, 2010, **20**, 256–275.
11 L. A. Bareford and P. W. Swaan, *Adv. Drug Delivery Rev.*, 2007, **59**, 748–758.
12 A. Verma and F. Stellacci, *Small*, 2010, **6**, 12–21.
13 A. Barchanski, U. Taylor, C. L. Sajti, L. Gamrad, W. A. Kues, D. Rath and S. Barcikowski, *J. Biomed. Nanotechnol.*, 2015, **11**, 1597–1607.
14 R. Weissleder, K. Kelly, E. Y. Sun, T. Shtatland and L. Josephson, *Nat. Biotechnol.*, 2005, **23**, 1418–1423.
15 A. Luchini, D. H. Geho, B. Bishop, D. Tran, C. Xia, R. L. Dufour, C. D. Jones, V. Espina, A. Patanarut, W. Zhou, M. M.

Ross, A. Tessitore, E. F. Petricoin III and L. A. Liotta, *Nano Lett.*, 2008, **8**, 350–361.

16 L. R. Khoury, R. Goldbart, T. Traitel, G. Enden and J. Kost, *ACS Nano*, 2015, **9**, 5750–5759.

17 S. Minardi, L. Pandolfi, F. Taraballi, X. Wang, E. De Rosa, Z. D. Mills, X. Liu, M. Ferrari and E. Tasciotti, *ACS Appl. Mater. Interfaces*, 2017, **17**, 14566–14575.

18 M. Liang, I. C. Lin, M. R. Whittaker, R. F. Minchin, M. J. Monteiro and I. Toth, *ACS Nano*, 2010, **4**, 403–413.

19 Z. J. Deng, M. Liang, I. Toth, M. J. Monteiro and R. F. Minchin, *ACS Nano*, 2012, **6**, 8962–8969.

20 C. A. Fustin, C. Colard, M. Filali, P. Guillet, A. S. Duwez, M. A. R. Meier, U. S. Schubert and J. F. Gohy, *Langmuir*, 2006, **22**, 6690–6695.

21 C. Rejeeth, T. C. Nag and S. Kannan, *Cancer Nanotechnol.*, 2013, **4**, 127–136.

22 L. Solhi, M. Atai, A. Nodehi, M. Imani, A. Ghaemi and K. Khosravi, *Dent. Mater.*, 2012, **28**, 369–377.

23 W. Zhang, J. Shen, H. Su, G. Mu, J. H. Sun, C. P. Tan, X. J. Liang, L. N. Ji and Z. W. Mao, *ACS Appl. Mater. Interfaces*, 2016, **8**, 13332–13340.

24 C. Rejeeth, R. Vivek and S. Kannan, *RSC Adv.*, 2015, **5**, 94534–94538.